

# BLENDING OF HYDROGEN INTO A NATURAL GAS DISTRIBUTION PIPELINE IN BRITISH COLUMBIA THROUGH A TEE JUNCTION FOR REDUCING GHG EMISSIONS

Arash J. Khabbazi<sup>1</sup>, Mojtaba Zabihi<sup>1</sup>, Ri Li<sup>1\*</sup> Matthew Hill<sup>2</sup>, Vincent Chou<sup>2</sup>, John Quinn<sup>2</sup>

<sup>1</sup>School of Engineering, University of British Columbia, Kelowna, BC, Canada, V1V1V7

<sup>2</sup>Renewable Gas Supply, FortisBC, Surrey, BC, Canada, V4N0E8

\*sunny.li@ubc.ca

**Abstract**—Integrating renewable hydrogen into the existing natural gas infrastructure network can reduce greenhouse gas (GHG) emissions and enhance electricity storage efficiency. To ensure a functional and durable network, attaining homogeneous mixing as quickly as possible is crucial. This study employs CFD analysis to evaluate hydrogen and methane mixing homogeneity in a pipeline with a vertical top-sided Tee junction. The coefficient of variation (CoV) of hydrogen mole fraction is analyzed along cross-sectional slices of a distribution pressure (DP) pipe where the ideal gas law is applicable due to low pressures. The findings reveal that reducing the diameter of the side pipe while maintaining the main pipe diameter results in a shorter mixing homogeneity length due to enhanced side flow jet penetration and increased diffusion. Notably, a sharp drop in the CoV figure is evidenced when reducing the side pipe from NPS 1.25 to NPS 1.0, leading to a substantial decrease in the mixing homogeneity length from 143 main pipe diameters from the branch center to 38 diameters.

**Keywords-component**—Grid decarbonization; Mixing homogeneity; Hydrogen; Natural gas; Equation of state; Coefficient of variation (CoV)

## I. INTRODUCTION

According to the Paris Agreement, all nations must take measures to reduce their greenhouse gas emissions (GHG) from all sources. The Canadian government has pledged to reach net-zero emissions by 2050 to prevent the negative impacts of climate change [1]. Given this, renewable and low-carbon gases such as green hydrogen and biomethane will be extremely important in the long run.

Hydrogen is called "green hydrogen" if it is created through renewable energy sources like solar cells and wind turbines. A comprehensive study regarding hydrogen production methods is conducted in [2]. Green hydrogen has great potential for reducing GHG emissions because of its carbon-free nature and production route. Additionally, it plays a crucial role in the

electricity sector. More specifically, the intermittent nature of renewable energy systems, including wind and solar, makes the power systems unstable and unreliable [3]. Therefore, the surplus electricity is converted through water electrolysis to green hydrogen, called Power-to-Gas (PtG) technology [4].

The obtained green hydrogen through PtG applications has to be delivered to the places of utilization. According to the [5], pipeline transmission outperforms truck delivery in places with high hydrogen demand. With rising production and consumption rates, it is plausible to imagine a fully-dedicated hydrogen infrastructure network. Given this and considering the current transition period, the most efficient solution is blending hydrogen into the existing natural gas grids, in which the two gaseous substances are transported as a new mixture.

The new fluid changes significantly in its transmission conditions because of the different thermophysical properties of hydrogen and natural gas. The changes also depend on the operating pressure of the network, ranging from high to low pressures. Therefore, care must be taken in determining the maximum amount of hydrogen within the grid, as it impacts the safety, durability, and integrity of the pipelines and customer equipment [6]. In British Columbia, Canada, the proposed hydrogen mole percentage within distribution pressure (DP) pipelines ranges from 5% to 20%. This study assumes a maximum hydrogen mole percentage of 20%.

The study of incorporating hydrogen into existing grids has drawn the attention of many researchers in the twenty-first century. Tabkhi [7] modeled a steady-state transmission-pressure (TP) case with several pipelines and compressor stations. An unsteady looped TP network was studied via the finite element method (FEM) in [8]. In another work, Uilhoorn [9] demonstrated that isothermal assumptions in transient high-pressure scenarios would lead to inaccuracies.

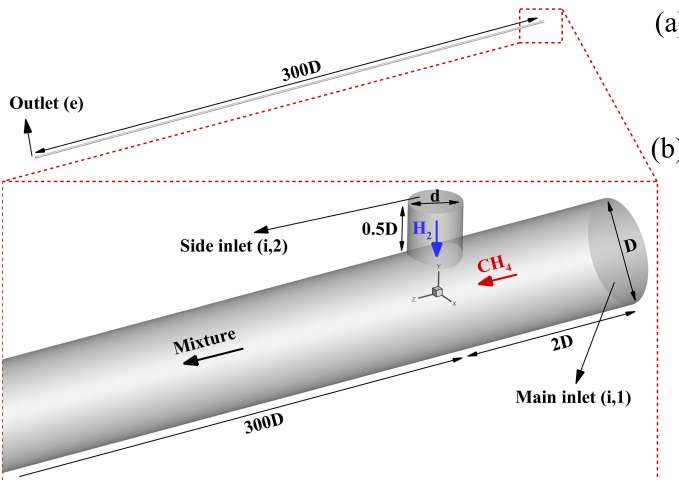


Figure. 1: A view of the entire pipe with a length of 302D (a) and its Tee junction (b).

As observed, existing studies primarily focus on modeling the transmission of uniform mixtures with specific hydrogen concentrations at high pressures, highlighting the need for further research on the hydrogen-natural gas mixing process in the pipelines, referred to as in-line mixing.

There are several in-line mixing options, including Tee junctions and static mixers, that can be utilized for single-phase turbulent flows [10]. Tee junctions prove to be an effective solution when the momentum of the side flow is sufficiently high. Eames [11] investigated a transmission pressure pipe equipped with a vertical Tee junction and showed that the injection rate, side pipe diameter, and injection location significantly affect the mixing process mainly due to a density contrast of eight times between hydrogen and methane. A deep neural network (DNN) model was developed in [12] to predict the mixing quality of hydrogen and natural gas in low-pressure bottom-sided Tee junctions. In another work, it was suggested that adding a static mixer, such as a helical static mixer, can improve the stratification of gases, resulting in a more uniform mixture [13]. The aim of this paper is to examine the effect of side stream momentum intensity on hydrogen and natural gas mixing by altering the pipe diameter in low-pressure scenarios where ideal gas conditions are met. Consequently, the mixing homogeneity (uniformity) length is also investigated. The mathematical details of the model are provided first. Consequently, the physical and computational details are presented. The simulation results are discussed in the results section before concluding the work.

## II. MATHEMATICAL FORMULATION

### A. Multi-species compressible turbulent flow model

The steady and dynamic flow behavior within a pipe is governed by conservation equations. The physical problem shown in Fig. 1 consists of a main pipeline with a side injection pipe, where the mixing occurs upon hydrogen injection through the side pipe. To analyze the mixing quality of two non-reacting gases, transport equations are required. The steady-state expressions with Einstein summation notation are

provided in the following, where the continuity equation is expressed as [14]:

$$\frac{\partial(\rho u_i)}{\partial x_i} = 0 \quad (1)$$

where  $\rho$  is density and  $u_i$  is the velocity magnitude. The momentum equation is given by

$$\frac{\partial(\rho u_i u_j)}{\partial x_j} = -\frac{\partial p}{\partial x_i} + \frac{\partial}{\partial x_j} \left[ \mu \left( \frac{\partial u_i}{\partial x_j} + \frac{\partial u_j}{\partial x_i} \right) \right] + \rho f_i \quad (2)$$

where  $p$  is pressure,  $\mu$  is dynamic viscosity, and  $f_i$  is the body force per unit volume, that is, the gravitational force acting on the flow in this problem. Derived from the first law of thermodynamics, the energy equation can be written as

$$\frac{\partial(\rho c_p u_j T)}{\partial x_j} = \frac{\partial}{\partial x_j} \left( k \frac{\partial T}{\partial x_j} \right) + u_j \frac{\partial p}{\partial x_j} + \mu \Phi \quad (3)$$

where  $T$  is temperature,  $c_p$  is the specific heat at constant pressure,  $k$  is thermal conductivity, and  $\Phi$  is the viscous dissipation function.

Introducing an equation of state (EoS) is crucial, as it links the density and other gas properties. At relatively low pressures, the gas components do not significantly influence one another and can be treated as ideal gases. Representing  $R$  as the mixture specific gas constant, ideal gas EoS is given by

$$p = \rho R T \quad (4)$$

Since gas mixing is a multi-species problem, an additional species transport equation is required to solve for the species mass fraction  $Y_i$  at different locations, given by [15]:

$$\frac{\partial(\rho u_j Y_i)}{\partial x_j} = \frac{\partial}{\partial x_j} \left[ \left( \rho D_{i,m} + \frac{\mu_t}{S_{Ct}} \right) \frac{\partial Y_i}{\partial x_j} \right] \quad (5)$$

where  $D_{i,m}$  is the mass diffusivity of the  $i_{th}$  component in the mixture or laminar diffusivity coefficient, which is a fluid property. The turbulent Schmidt number is  $S_{Ct} = \mu_t / \rho D_t$  taken as 0.7, where  $\mu_t$  is the turbulent viscosity, and  $D_t$  is the turbulent diffusivity, which is a turbulent flow characteristic. In turbulent flow conditions,  $D_{i,m}$  is generally not important, as the effective diffusivity  $D_{eff}$  is dominated by  $D_t$ . It should be noted that for a multi-component mixture,  $\sum_{i=1}^n Y_i$  is always unity. Therefore, solving (5) for one of the species is sufficient in binary mixtures, as  $Y_1 + Y_2 = 1$  relates both to one another.

As the pressure increases in the pipe, turbulent mixing becomes a critical flow characteristic due to the large Reynolds numbers of the main and side flows. Depending on the application and computational resources, various turbulence models have been implemented in the literature. The  $k - \epsilon$  model [16] is particularly useful when the turbulent length scale is much greater than the molecular length scale, e.g., pipe flows. Two additional transport equations for the turbulence kinetic energy  $k$  and its dissipation rate  $\epsilon$  should be defined accordingly. In this paper, the realizable  $k - \epsilon$  model [17] is implemented as it has shown improved performance in a wide range of flows.

### B. Thermodynamic mixture relations

Equation (4) for ideal gases is a crucial factor for analyzing compressible flows. To accurately analyze the mixtures, proper relations between components and the mixture should be established. The previously defined  $R$  in (4) is defined for a single component as outlined in [18]:

$$R_i = \frac{\bar{R}}{M_i} \quad (6)$$

where  $\bar{R}$  is universal gas constant, and  $R_i$  and  $M_i$  denote specific gas constant and molar weight for the  $i_{th}$  component, respectively.

The ideal gas specific heat at constant pressure for each component  $c_{p,i}$  is defined as

$$c_{p,i}(T) = c_{p,1} + c_{p,2}T + c_{p,3}T^2 + c_{p,4}T^3 + c_{p,5}T^4 \quad (7)$$

where the constants  $c_{p,1}$ ,  $c_{p,2}$ ,  $c_{p,3}$ ,  $c_{p,4}$ , and  $c_{p,5}$  are defined in [19].

The enthalpy  $h_i$  and entropy  $s_i$  of each component can be expressed as

$$h_i(T) = \int_{T_0}^T c_{p,i}(T) dT + h_{i,0}(T_0) \quad (8)$$

$$s_i(T, p) = \int_{T_0}^T \frac{c_{p,i}(T)}{T} dT + R \ln \frac{p_0}{p} + s_{i,0}(T_0, p_0) \quad (9)$$

where the variables with 0 subscripts represent the reference state conditions.

The temperature-dependant dynamic viscosity of the  $i_{th}$  component is described by [20]:

$$\mu_i(T) = 6.3 \times 10^{-7} \frac{M_i^{1/2} (p_{cr,i}/p_{atm})^{2/3}}{T_{cr,i}^{1/6}} \left( \frac{T_{r,i}^{3/2}}{T_{r,i} + 0.8} \right) \quad (10)$$

where  $P_{cr,i}$  is the critical pressure of the  $i_{th}$  component,  $p_{atm}$  is the standard pressure 101.325 kPa,  $T_{cr,i}$  is the critical temperature of the  $i_{th}$  component, and the reduced temperature is  $T_{r,i} = T/T_{cr,i}$ . Given this, the thermal conductivity of each component is [21]:

$$k_i = \mu_i \left( c_{p,i} + \frac{10.4}{M_i} \right) \quad (11)$$

Using a linear mixing rule, the properties of the mixture and a single component relates by

$$\psi = \sum_{i=1}^n Y_i \psi_i \quad (12)$$

where  $\psi$  can be replaced by  $R$ ,  $c_p$ ,  $h$ ,  $s$ ,  $\mu$ , and  $k$  and stands for a mixture property, and  $\psi_i$  denotes that of a single component. The mole fraction  $x_i$  relates to the mass fraction  $Y_i$  through  $x_i = Y_i M/M_i$ .

### C. Boundary conditions

The geometry consists of two inlets and one outlet. Given a specific mass flow rate in the main pipe, the mole flow rate can be found by

$$\dot{n} = \frac{\dot{m}}{M} \quad (13)$$

Through the total mole conservation and hydrogen mole conservation in the system

$$\overline{x_{H_2,e}} = \frac{\dot{n}_{i,2}}{\dot{n}_{i,1} + \dot{n}_{i,2}} \quad (14)$$

where 'i,1', 'i,2', and 'e' denote the main inlet, side inlet, and outlet conditions, respectively. Given the linearity of the ideal gas EoS, (14) can be further simplified. Rewriting (4) on a molar basis and applying (13) to it leads to

$$\dot{n} = \frac{p \dot{V}}{RT} \quad (15)$$

where the volumetric flow rate is  $\dot{V} = \rho \dot{m}$ . Combining (14) and (15) gives

$$\overline{x_{H_2,e}} = \frac{1}{1 + \frac{p_{i,1}}{p_{i,2}} \frac{T_{i,2}}{T_{i,1}} \frac{\dot{V}_{i,1}}{\dot{V}_{i,2}}} \quad (16)$$

which relates inlet properties and the average hydrogen mole fraction at the outlet.

Assuming a radially constant density at the inlets, a power-law profile for the fully-developed mass flux at both inlets is defined by

$$\overline{j_m} = \left( \frac{n+1}{n} \right) \left[ 1 - \left( \frac{r}{r_p} \right)^m \right]^{\frac{1}{n}} \quad (17)$$

where  $j_m$  is the mass flux,  $\overline{j_m}$  is the average mass flux,  $r_p$  is pipe radius,  $r$  is the radial distance from the inlet face center, and the coefficients  $m$  and  $n$  are chosen such that the fitting matches the experimental profiles, which are set to 2 and 7, respectively [22].

In a highly-turbulent flow, defining an appropriate turbulent intensity (TI) is important. However, it is challenging to set an exact TI profile, which necessitates using an average value. Basse [23] showed that an area-averaged (AA) power-law fit has the closest correlation with the experimental data in [24]. Therefore

$$I_{AA} = 0.3173 \times Re_D^{-0.1095} \quad (18)$$

where  $I_{AA}$  is the area-averaged turbulence intensity and  $Re_D$  is the flow Reynolds number in the pipe.

### D. Quantifying the mixing homogeneity

The coefficient of variation (CoV) is a quantity for measuring the intensity of segregation and is widely used for assessing the mixing homogeneity [25]. It is derived from the ratio of the standard deviation of the concentration data to the mean concentration measurements. In this context, the mole fraction is used instead of mole concentration because it provides a better measure for relative proportions of the components, regardless of the mixture pressure or temperature. Thus, the CoV is defined on each cross-section along the main pipe,

$$CoV = \frac{1}{\overline{x_{H_2}}} \sqrt{\frac{1}{A} \int_A (x_{H_2} - \overline{x_{H_2}})^2 dA} \quad (19)$$

where  $x_{H_2}$  is the hydrogen mole fraction on different points on each cross-section,  $\overline{x_{H_2}}$  is the average hydrogen mole

fraction on each cross-section, and the cross-section area is  $A = \pi D^2/4$ . In industrial processes, a CoV between 0.5% and 5% typically indicates a uniformly distributed mixture [10]. Thus, for the proper functioning of end-user devices, a more stringent value of 1.5% is selected as the standard in this study to ensure a homogeneous mixture.

### III. COMPUTATIONAL DETAILS

#### A. Case description

A distribution pressure (DP) NPS 6 pipe with an inner diameter (ID)  $D$  of 6.065 inches and a length  $L$  of 302D exiting a gate station is considered. 302D for this line is approximately 46 meters, which is where the first branch in the downstream distribution network is located. Thus, it is a good representation of the maximum length  $L$  where homogeneous mixing is necessary. The standard terminology "NPS" refers to nominal pipe size and gives an approximate indication of ID at small pipe diameters [26]. In this work, all pipes have been assigned a standard wall thickness of STD or 40s, where "Sch." denotes Schedule, a standard for pipe wall thickness. In order to reflect actual pipe sizes commonly used in industry, eight side pipe cases ranging from NPS 0.5 to NPS 3.0 have been chosen. The flow rate and other gas properties vary throughout the year, from low consumption in summer to high consumption in winter. In this study, the operating distribution pressure is 420 kPa, which is reduced from a maximum transmission pressure of 6.62 MPa within the station. Inlet pressures are almost equal, as there is negligible pressure drop due to short entry lengths. The temperatures of the main and side flows are set to 276.5 K and 288.15 K, respectively. An average mass flow rate of  $0.5 \text{ kg s}^{-1}$  moves through the main pipe. Knowing the average hydrogen mole fraction within the system and the flow rate at the main pipe, the side pipe flow rate can be determined from (16). To simplify, natural gas with a methane composition of over 90% is treated as pure methane. Therefore, the density contrast of almost eight times in ideal gas conditions originates from the different molar weights of methane  $M_{CH_4} = 16.04303 \text{ kg kmol}^{-1}$  and  $M_{H_2} = 2.01594 \text{ kg kmol}^{-1}$ . Given these, the problem reduces to a two-species, single-phase model.

#### B. Computational domain

The mesh generation is performed by Fluent meshing software to generate a polyhedral grid throughout the domain (Fig. 2). Polyhedral meshes conform to complex geometries, easily adapting to changing flow conditions. Besides significantly saving computational expenses, they provide reasonable accuracy. The origin of the Cartesian coordinate system is placed at the center of the junction.

To assess the sensitivity of the simulation results to the mesh resolution, a grid study is performed for the base case, with a length of 300D, a main pipe of NPS 6, and a side pipe of NPS 3. Five cases with different cell numbers are studied accordingly. The upper wall friction factor, the hydrogen mole fraction on the upper surface, and the velocity magnitude on

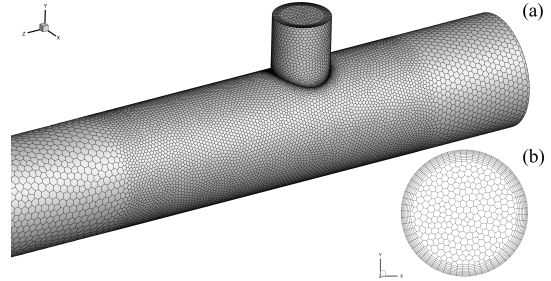


Figure 2: 3-D branch view (a) and cross-sectional main pipe view (b) of the computational grid.

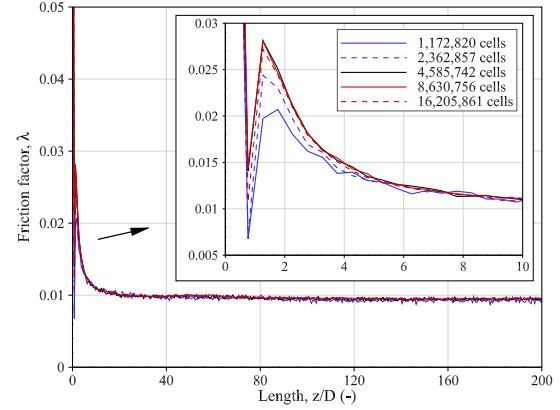


Figure 3: Main pipe upper surface friction factor for different cases.

the centerline are tested to confirm the grid study accuracy. The results for the wall friction factor are shown in Fig. 3.

Fig. 3 shows that the top wall friction factor is not consistent initially, but the lines fit on one another after some distance from the injection point. This is because the side flow jet penetrates the main flow at the intersection, strong vortices and rotations are expected. To overcome this, a denser mesh is used 1D upstream and 2D downstream of the branch center, as demonstrated in Fig. 2. The mean absolute percentage error (MAPE) for hydrogen mole fraction, velocity magnitude, and friction factor between 8,630,756 and 4,585,742 cells is in an acceptable range compared to other cases. Therefore, 4,585,742 cells case is chosen for efficiency.

#### C. Numerical discretization

The numerical analysis is performed via ANSYS Fluent 2020 R2, a commercial CFD software package. The coupled method, which solves for both the velocity and pressure fields simultaneously, was employed. It outperforms a segregated method in robustness and accuracy, especially in a compressible flow case. The second-order spatial discretization method was used everywhere. To track the species of methane and hydrogen, the species transport model with no volumetric reactions was utilized. Owing to the inadequate computing performance of Fluent in applying EoS to mixtures [27], a user-defined ideal gas EoS for the mixture of hydrogen and methane was developed and compiled into Fluent separately. The realizable  $k - \epsilon$  turbulence model with full buoyancy effects was implemented.

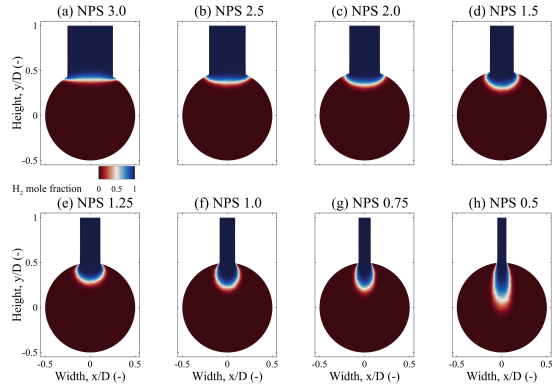


Figure 4: Cross-sectional view of hydrogen distribution at the branch center ( $z = 0$ ) for different side pipes (a-h). The dimensions are shown in terms of the main pipe diameter  $D$  for a better representation.

#### IV. RESULTS

Fig. 4 depicts a cross-sectional view ( $z$  slice) of hydrogen distribution at the branch center ( $z = 0$ ) for all eight side pipes. It can be seen that the intensity of jet penetration increases as the side pipe diameter decreases. Since the side pipe mass flow rate is kept constant in all cases, reducing its diameter increases the momentum flux. This increase in momentum leads to a heightened jet penetration.

Moving one main pipe diameter downstream of the flow, as shown in Fig. 5, a low side stream momentum causes it to deflect when it comes to contact with the main flow. This is confirmed by observing the first five cases in Fig. 5(a-e), where hydrogen is trapped near the upper surface of the pipe, indicating poor mixing quality. This is similar to an empty or coaxial pipe scenario, where simple mixing occurs due to turbulence eddies promoting axial and radial mass interchange. On the other hand, the mixing is expected to improve significantly in the last three cases in Fig. 5(f-h), where the side stream penetrates deeply into the bulk flow.

Upon blending the hydrogen, its velocity suddenly gets accelerated in the main flow direction, eventually reaching the main flow velocity. The significant density difference between hydrogen and methane causes hydrogen to be buoyant and get trapped in the vicinity of the upper surface. This is observed in Fig. 6, where the mixing progression downstream of the pipe after 10D is demonstrated. The final three cases in Fig. 6(f-h) are almost reached homogeneity, whereas the first five cases in Fig. 6(a-e) still exhibit the dark red color (zero mole%) for hydrogen mole fraction in the vicinity of the lower wall.

To evaluate the mixing homogeneity quantitatively, the previously defined expression for CoV in (19) is used. The hydrogen mole fraction is found on three lines along the pipe on the upper surface, center line, and lower surface. To clarify, the smallest (NPS 0.5) and greatest (NPS 3.0) side pipe diameters are compared. Fig. 7 indicates that the mixing homogeneity length for the former is 34D, while it is 159D for the latter, confirming its reduction by decreasing the side pipe diameter.

Fig. 8 compares the CoV versus the dimensionless length  $z/D$  for all cases and confirms the previous observations. That

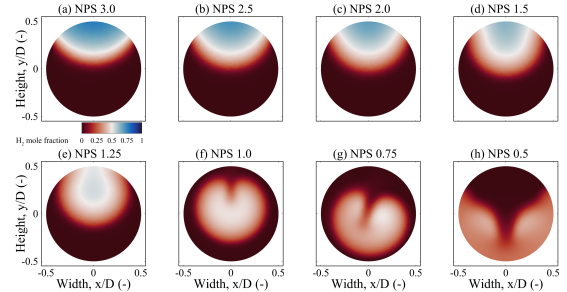


Figure 5: Cross-sectional view of hydrogen mole fraction after 1D from the injection location (a-h).

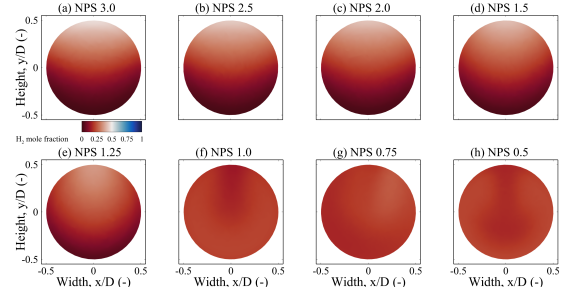


Figure 6: Cross-sectional view of hydrogen distribution after 10D from the injection point (a-h).

is to say, the curves become much steeper as the side pipe diameter decreases, indicating that the mixing homogeneity length reduces. A notable gap in Fig. 8 is also observed between NPS 1.0 and NPS 1.25 cases, showing that the three pipes with the least sizes achieve homogenization in significantly shorter lengths. This finding is consistent with previous explanations. In the first five cases, hydrogen remains along the upper surface due to buoyancy forces, giving rise to a stratified flow of methane and hydrogen for a distance after the injection. Therefore, turbulent diffusion plays a crucial role in driving the mixing process in the final stages. However, the side flow momentum flux is significantly increased in the last three cases, where buoyancy forces tend to elevate the hydrogen flow simultaneously, significantly improving the mixing process.

As demonstrated in Fig. 5(f) and 5(g), the introduced hydrogen diffuses from all directions due to an extended contact time created by the heart-shaped distribution pattern. In Fig. 5(a-e), however, it tended to diffuse only from the lower side that was in direct contact with the main flow. As illustrated in Fig. 5(h), the side stream collides with the lower inner surface

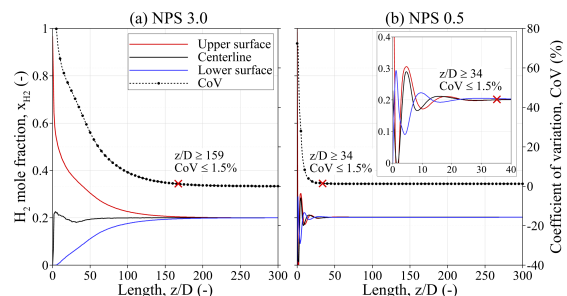


Figure 7: CoV and Hydrogen mole fraction variation on different cross-sections along the pipe

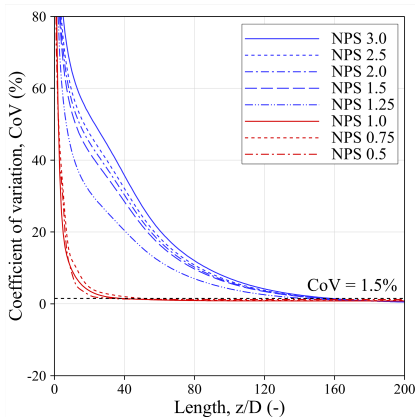


Figure. 8: The comparison of CoV variation on different cross-sections along the pipe for all cases.

of the pipe, where hydrogen is diverted and flows up along the inner wall of the pipe. As a result, turbulent mixing increases significantly. Generally, the side stream momentum must be adequately high to achieve distributive mixing. However, it is crucial to prevent it from becoming too high, as backmixing would occur. Besides, increasing the velocity of the hydrogen can lead to higher noise levels, making it necessary to be cautious of practical velocity limits for injections in above-grade pipes, with a maximum recommended velocity of 30 m/s. Therefore, balancing the need for efficient mixing with practical considerations is vital.

## V. CONCLUSION

A computational study for the turbulent mixing of hydrogen and methane non-reacting gases in different Tee junctions was carried out in this work. The simulation was performed on ANSYS Fluent through user-defined ideal gas EoS, considering low-pressure conditions in the distribution network. The impact of changing the side pipe diameter in the mixing homogeneity length is analyzed quantitatively using CoV for hydrogen mole fraction. The findings suggest that the side pipe jet penetration plays an important role in determining the mixing homogeneity length of gases. It has been observed that the homogeneity length decreases by reducing the side pipe diameter. The reduction was significant from NPS 1.25 to NPS 1.0 because the side flow interacts with the bottom surface of the main pipe, and a chaotic mixing occurs. Besides, the contact time increases, and diffusion strongly affects the mixing process. Our future work mainly focuses on mixing in intermediate pressure (IP) and transmission pressure (TP) cases, where using real gas equations of state will be inevitable. An analytical study is needed to understand better the relations between non-dimensionless parameters that govern the mixing process. Additionally, further study is required for the buoyancy impact of hydrogen for different injection arrangements, i.e., vertical distribution line vs. the horizontal line modeled here.

## REFERENCES

- [1] Government of Canada, Canadian Net-Zero Emissions Accountability Act. 2021.
- [2] I. Dincer and C. Acar, "Review and evaluation of hydrogen production methods for better sustainability," *Int. J. Hydrogen Energy*, vol. 40, no. 34, pp. 11094–11111, Sep. 2014, doi: 10.1016/j.ijhydene.2014.12.035.
- [3] M. Peker, A. S. Kocaman, and B. Y. Kara, "Benefits of transmission switching and energy storage in power systems with high renewable energy penetration," *Appl. Energy*, vol. 228, pp. 1182–1197, Oct. 2018, doi: 10.1016/j.apenergy.2018.07.008.
- [4] M. Lehner, R. Tichler, H. Steinmüller, and M. Koppe, *Power-to-gas: Technology and business models*. Springer International Publishing, 2014.
- [5] C. Yang and J. Ogden, "Determining the lowest-cost hydrogen delivery mode," *Int. J. Hydrogen Energy*, vol. 32, no. 2, pp. 268–286, Feb. 2007, doi: 10.1016/j.ijhydene.2006.05.009.
- [6] M. Melaina, O. Antonia, and M. Penev, "Blending hydrogen into natural gas pipeline networks: A review of key issues," 2013, doi: 10.2172/1068610.
- [7] F. Tabkhi, C. Azzaro-Pantel, L. Pibouleau, and S. Domenech, "A mathematical framework for modelling and evaluating natural gas pipeline networks under hydrogen injection," *Int. J. Hydrogen Energy*, vol. 33, no. 21, pp. 6222–6231, Nov. 2008, doi: 10.1016/j.ijhydene.2008.07.103.
- [8] Z. Hafsi, S. Elaoud, and M. Mishra, "A computational modelling of natural gas flow in looped network: Effect of upstream hydrogen injection on the structural integrity of gas pipelines," *J. Nat. Gas Sci. Eng.*, vol. 64, pp. 107–117, Apr. 2019, doi: 10.1016/j.jngse.2019.01.021.
- [9] F. E. Uilhoorn, "Dynamic behaviour of non-isothermal compressible natural gases mixed with hydrogen in pipelines," *Int. J. Hydrogen Energy*, vol. 34, no. 16, pp. 6722–6729, Aug. 2009, doi: 10.1016/j.ijhydene.2009.06.062.
- [10] A. W. Etchells and C. F. Meyer, "Mixing in Pipelines," in *Handbook of Industrial Mixing*, John Wiley Sons, Ltd, 2004, pp. 391–477.
- [11] I. Eames, M. Austin, and A. Wojcik, "Injection of gaseous hydrogen into a natural gas pipeline," *Int. J. Hydrogen Energy*, Jun. 2022, doi: 10.1016/J.IJHYDENE.2022.05.300.
- [12] Y. Su, et al., "Prediction of Mixing Uniformity of Hydrogen Injection in Natural Gas Pipeline Based on a Deep Learning Model," *Energies*, vol. 15, no. 22, pp. 8694, Nov. 2022, doi: 10.3390/EN15228694.
- [13] M. Kong, S. Feng, Q. Xia, C. Chen, Z. Pan, and Z. Gao, "Investigation of mixing behavior of hydrogen blended to natural gas in gas network," *Sustain.*, vol. 13, no. 8, p. 4255, Apr. 2021, doi: 10.3390/su13084255.
- [14] F. White, *Viscous Fluid Flow*, 3rd ed. McGraw-Hill Mechanical Engineering, 2005.
- [15] A. Bejan, *Convection heat transfer*, 4th ed. Wiley, 2013.
- [16] B. E. Launder and D. B. Spalding, *Lectures in Mathematical Models of Turbulence*, Academic Press, London, England, 1972.
- [17] T.-H. Shih, W. W. Liou, A. Shabbir, Z. Yang, and J. Zhu, "A New  $k-\epsilon$  Eddy-Viscosity Model for High Reynolds Number Turbulent Flows - Model Development and Validation". *Computers Fluids*. 24(3). 227–238. 1995.
- [18] C. (Claus) Borgnakke and R. E. Sonntag, *Fundamentals of thermodynamics*, 8th ed. 2012.
- [19] M. J. Moran and H. N. Shapiro, "Fundamentals of Engineering Thermodynamics," John Wiley Sons, Inc., 1988.
- [20] N. P. Cheremisinoff. *Fluid Flow Pocket Handbook*. Gulf Publishing Company. Houston, TX, 1984.
- [21] E. R. G. Eckert and R. M. Drake. *Analysis of Heat and Mass Transfer*. McGraw-Hill Company. 1972.
- [22] A. Salama, "Velocity Profile Representation for Fully Developed Turbulent Flows in Pipes: A Modified Power Law," *Fluids* 2021, Vol. 6, Page 369, vol. 6, no. 10, p. 369, Oct. 2021, doi: 10.3390/FLUIDS6100369.
- [23] N. T. Basse, "Turbulence intensity scaling: A fugue," *Fluids*, vol. 4, no. 4, p. 180, Oct. 2019, doi: 10.3390/fluids4040180.
- [24] M. Hultmark, M. Vallikivi, S. C. C. Bailey, and A. J. Smits, "Turbulent pipe flow at extreme reynolds numbers," *Phys. Rev. Lett.*, vol. 108, no. 9, p. 094501, Feb. 2012, doi: 10.1103/PhysRevLett.108.094501.
- [25] A. Kukuková, B. Noël, S. M. Kresta, and J. Aubin, "Impact of sampling method and scale on the measurement of mixing and the coefficient of variance," *AICHE J.*, vol. 54, no. 12, pp. 3068–3083, Dec. 2008, doi: 10.1002/aic.11639.
- [26] ASME, ASME B36.19M-2018: Stainless Steel Pipe. ASME, 2018.
- [27] X. Liu, G. Michal, A. Godbole, and C. Lu, "Decompression modelling of natural gas-hydrogen mixtures using the Peng-Robinson equation of state," *Int. J. Hydrogen Energy*, vol. 46, no. 29, pp. 15793–15806, Apr. 2021, doi: 10.1016/j.ijhydene.2021.02.129.